JAMES WEBB SPACE TELESCOPE FUEL SLOSH ESTIMATION

Thi-han W. Nge[*], Matthew M. Wittal[†], Carl Hansen[‡], and Peter Gauthier[§]

The mitigation of fuel slosh in microgravity environments is a pressing matter for the control of both manned and unmanned spacecraft. This paper investigates the attitude perturbations caused by fuel slosh aboard the James Webb Space Telescope (JWST). We develop a dynamical model to parse these perturbations from slew telemetry data. This model uses special Euclidean group $\mathsf{SE}(3)$ as well as a novel, N-body variational integrator. The enhanced ability to validate fuel slosh models offers the reduction of settling time after slew operations and, accordingly, the maximization of available science time.

INTRODUCTION

The Artemis program will require spacecraft to perform rendezvous, proximity operations, and docking (RPOD) while carrying unprecedented quantities of fuel [1, 2]. The Human Landing Systems (HLS) in development by Blue Origin, Dynetics, and SpaceX each call for several refueling missions in orbit. As fuel is burned and volume is freed within a spacecraft's tanks, a large range of slosh modes and excitation frequencies must be considered. As such, fuel slosh can present a major complication to the guidance, navigation, and control (GN&C) of a spacecraft [3]. Accordingly, the models created to represent microgravity fuel slosh can be complex and as of the time of writing none have been successfully validated by on-orbit data. Logistical and operational constraints, such as the budgeting of spacecraft time, propellant budget, and upmass, can hinder validation efforts. The analysis of slew telemetry data for the purpose of fuel slosh estimation promises the validation of fuel slosh models without interruption to the spacecraft's science mission.

Another important application of fuel slosh mitigation is that of space telescopes, which often have stringent pointing requirements. The James Webb Space Telescope (JWST), launched on December 25, 2021, carries approximately 150 kg of hypergolic propellants to maintain its unstable orbit around the Sun-Earth Lagrange 2 (L2) point. The JWST also requires a pointing accuracy of > 1 arcsecond to its science target before fine guidance can begin. In this paper, an algorithm is developed to perform fuel slosh estimation for JWST using slew telemetry data provided by the Space Telescope Science Institute (STScI). An N-body, 6-DoF dynamical model is developed to simulate the attitude perturbations expected for the JWST in orbit. This simulated attitude data may

[*]Student, Department of Ocean and Mechanical Engineering, Florida Atlantic University, 777 Glades Rd, Boca Raton, FL 33431

[†]Automation and Robotics Systems Engineer, Granular Mechanics and Regolith Operations Laboratory, NASA Kennedy Space Center, FL 32899, and Ph.D. Candidate, Embry-Riddle Aeronautical University, 1 Aerospace Blvd., Daytona Beach, FL 32114

[‡]JWST Spacecraft Systems Engineer, SEITO Flight Systems Engineering Branch, Space Telescope Science Institute, 3700 San Martin Drive, Baltimore, MD 21218

[§]JWST Principal Flight Systems Engineer, Flight Systems Engineering Branch, Space Telescope Science Institute, 3700 San Martin Drive, Baltimore, MD 21218

then be compared with recorded attitude data in the form of slew telemetry. The formulation of these algorithms on Lie group $\mathsf{SE}(3)$ enables the consideration of orbit-attitude coupling without the singularities, unwinding, or nonuniqueness issues present in other attitude parameterization sets [4].

FORMULATION ON SPECIAL EUCLIDEAN GROUP $\mathsf{SE}(3)$

The pose of a rigid body is expressed in $\mathsf{SE}(3)$ as

$$g = \begin{bmatrix} R & r \\ 0_{1\times 3} & 1 \end{bmatrix} \in \mathsf{SE}(3) \tag{1}$$

where $R \in \mathsf{SO}(3)$ is the rotation matrix from the body frame $\mathcal{B}$ to the inertial frame $\mathcal{N}$ and r is the position vector in the inertial frame. The rigid body's velocity can be defined using an augmented velocity vector $\mathbb{V}$ as

$$\mathbb{V} = \left[\omega^T, v^T\right]^T \in \mathbb{R}^6 \tag{2}$$

such that $\omega \in \mathbb{R}^3$ is the angular velocity in the body frame $\mathcal{B}$ and $v \in \mathbb{R}^3$ is the translational velocity relative to the inertial frame and expressed in the body frame. The dynamic equations for a rigid body with can be expressed in $\mathsf{TSE}(3)$ as

$$\dot{g} = g\mathbb{V}^{\vee} \tag{3}$$

$$\dot{\mathbb{V}} = \mathbb{I}^{-1}\left(\mathrm{ad}^*_{\mathbb{V}}\mathbb{I}\mathbb{V} + \tau + u\right) \tag{4}$$

where $\tau \in \mathbb{R}^6$ are external torques and forces acting on the rigid body. and $u \in \mathbb{R}^6$ are control inputs. The augmented inertia tensor $\mathbb{I}$ can be defined as

$$\mathbb{I} = \begin{bmatrix} J & 0_{3\times 3} \\ 0_{3\times 3} & mI_3 \end{bmatrix} \in \mathbb{R}^{6\times 6}, \tag{5}$$

such that $I_3 \in \mathbb{R}^{3\times 3}$ is an identity matrix and the coadjoint operator is defined as

$$\mathrm{ad}^*_{\mathbb{V}} = \mathrm{ad}^T_{\mathbb{V}} = \begin{bmatrix} -\omega^{\times} & -v^{\times} \\ 0_{3\times 3} & -\omega^{\times} \end{bmatrix} \in \mathbb{R}^{6\times 6} \tag{6}$$

DYNAMICAL MODEL

The dynamical model is responsible for calculating the differential states $\dot{g}$ and $\dot{\mathbb{V}}$ using equations 3 and 4 respectively. Here, phenomena such as gravitational attraction, solar radiation pressure, and gravity gradient torque are considered.

Development of an N-Body Variational Integrator

The integrator is responsible for propagating state information forward through time. Numerical integrators (NI) are first-order accurate, whereas variational integrators (VI) are second-order accurate [4]. This makes VI's especially well-suited for the problem of nonlinear dynamics.

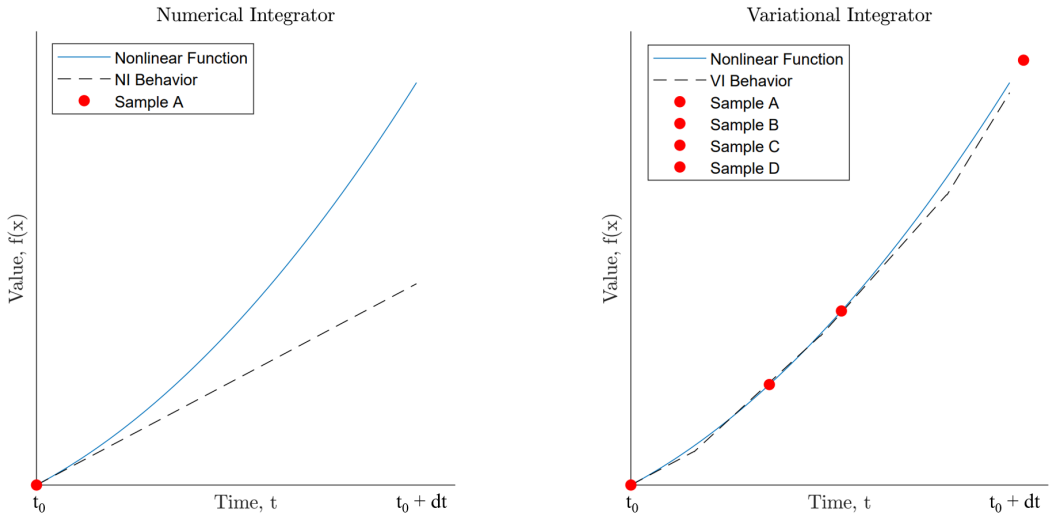

Figure 1. NI versus VI behavior for one timestep of a nonlinear function.

Figure 1 shows the performance of an NI versus that of a VI for a sample second-order equation. The x-axis spans one timestep for both graphs. By sampling the differential function four times per timestep, the VI achieves a much more accurate propagation. It is worth noting that the nonlinear function, shown here as $f(x)$, is not necessarily a function of time. Instead, it varies over time according to a differential function $\frac{\mathrm{d}f(x)}{\mathrm{d}t}$. As such, the distribution of sample points A, B, C, and D throughout the timestep merely reflects the time at which $f(x)$ and therefore $\frac{\mathrm{d}f(x)}{\mathrm{d}t}$ would match that of the propagated point.

Traditionally, a VI can only propagate the state of one body at a time. An N-body simulation requires the other bodies to be propagated using an NI. The effects of this are twofold. Firstly, the NI may struggle to capture the nonlinear dynamics of these other bodies. Secondly, the influence of our spacecraft on these other bodies and vice versa is treated as negligible. For this paper, the VI has been reworked to accept n-bodies through the modification of its matrix operations.

As seen in Algorithm 1, the VI calls the dynamical model and performs successive propagation of the differential state. It then updates the states by propagating a weighted average of the recorded differential states.

NUMERICAL SIMULATION

Initial states for the 11 bodies were generated using ephemeris data from the JPL Horizons system, corresponding to A.D. 2023-Aug-01 00:00:00.0000 TDB. Figure 2 and 3 show the VI output for the JWST.

Figure 2 shows that the simulated JWST position matches ephemeris data to within 0.67 m, with

Algorithm 1 Variational Integrator Logic

Initializing:

Define Initial Conditions $g_0, \mathbb{V}_0$

Begin Main Iteration Loop:

for $t = 1, 2, ...$ **do**

1: Call Dynamical Model at Point A
$[\dot{g}_a, \dot{\mathbb{V}}_a] = f(g_0, \mathbb{V}_0)$
2: Propagate Differential States for $\frac{1}{2}$ Timestep to Point B
$[g_b, \mathbb{V}_b] = h(g_0, \mathbb{V}_0, \dot{g}_a, \dot{\mathbb{V}}_a, \frac{1}{2}dt)$
3: Call Dynamical Model at Point B
$[\dot{g}_b, \dot{\mathbb{V}}_b] = f(g_b, \mathbb{V}_b)$
4: Propagate Differential States for $\frac{1}{2}$ Timestep to Point C
$[g_c, \mathbb{V}_c] = h(g_0, \mathbb{V}_0, \dot{g}_b, \dot{\mathbb{V}}_b, \frac{1}{2}dt)$
5: Call Dynamical Model at Point C
$[\dot{g}_c, \dot{\mathbb{V}}_c] = f(g_c, \mathbb{V}_c)$
6: Propagate Differential States for 1 Timestep to Point D
$[g_d, \mathbb{V}_d] = h(g_0, \mathbb{V}_0, \dot{g}_c, \dot{\mathbb{V}}_c, dt)$
7: Call Dynamical Model at Point D
$[\dot{g}_d, \dot{\mathbb{V}}_d] = f(g_d, \mathbb{V}_d)$
8: Propagate Differential States for 1 Timestep and Store Values
$[g_t, \mathbb{V}_t] = h(g_0, \mathbb{V}_0, (\frac{1}{6}\dot{g}_a, \frac{1}{3}\dot{g}_b, \frac{1}{3}\dot{g}_c, \frac{1}{6}\dot{g}_d), (\frac{1}{6}\dot{\mathbb{V}}_a, \frac{1}{3}\dot{\mathbb{V}}_b, \frac{1}{3}\dot{\mathbb{V}}_c, \frac{1}{6}\dot{\mathbb{V}}_d), dt)$
9: Update States
$[g_0, \mathbb{V}_0] = [g_t, \mathbb{V}_t]$

end

respect to the International Celestial Reference Frame (ICRF), over a span of 25000 sec. Figure 3 shows attitude perturbations on the order of 1×10^{-7} rad/s produced by the orbit-attitude coupling of $\mathsf{SE}(3)$.

Telemetry Data

The data shown in Figure 4 and 5 correspond to the settling time after a coarse slew maneuver conducted on A.D. 2023-Aug-10 11:42:44.2380 UTC.

The unfiltered A-STR star tracker attitude data shown in Figure 4 shows low frequency attitude perturbations after the completion of the course slew. Figure 5 shows the body torque commanded by the spacecraft's control system to counter these attitude perturbations. This data constitutes control input *u* fed to the dynamical model.

EXPECTED RESULTS

An N-body variational integrator has been developed for the problem of estimating fuel slosh for the James Webb Space Telescope. This VI references a dynamical model to simulate the motion of the JWST in 6-DoF to allow for the comparison of its attitude perturbations with recorded slew telemetry data. The benefits of this work include enhanced methods of simulating nonlinear systems, and the final paper will demonstrate how nonlinear motion may be extracted from noisy data. This may be especially worthwhile for simulating the rendezvous, proximity operations, and

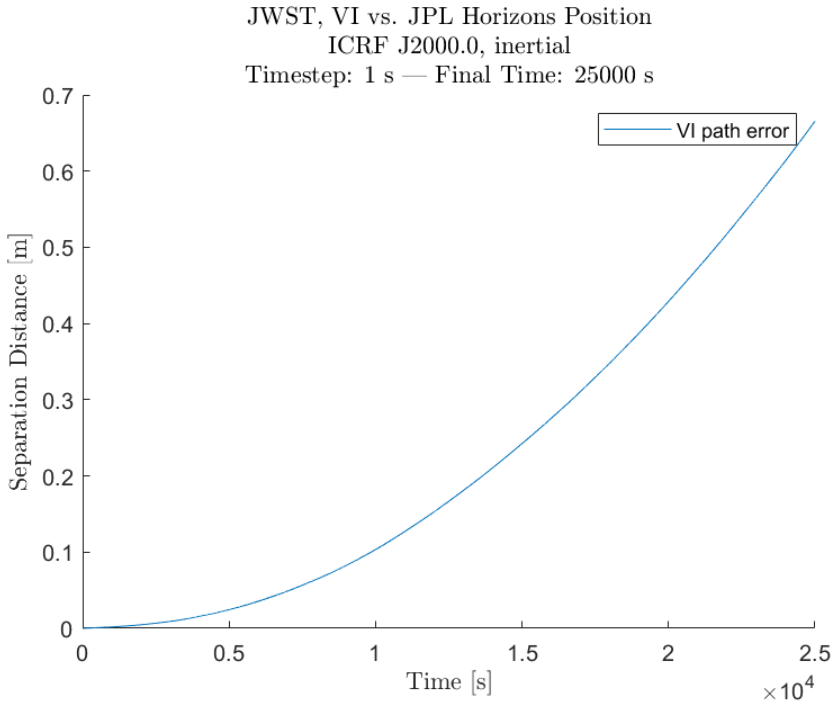

Figure 2. Position error of the JWST VI output versus JWST JPL Horizons ephemeris.

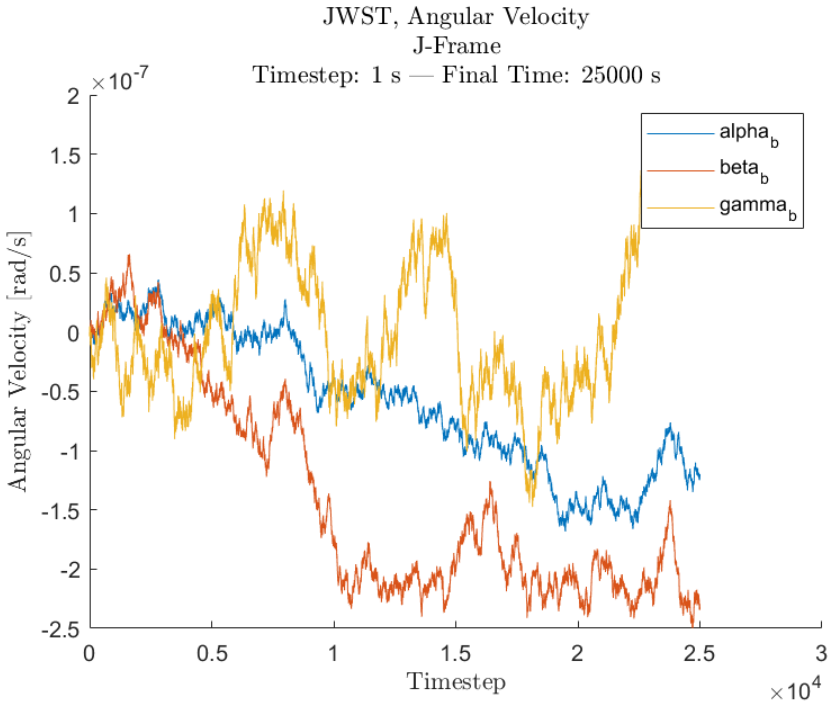

Figure 3. JWST VI angular velocity output.

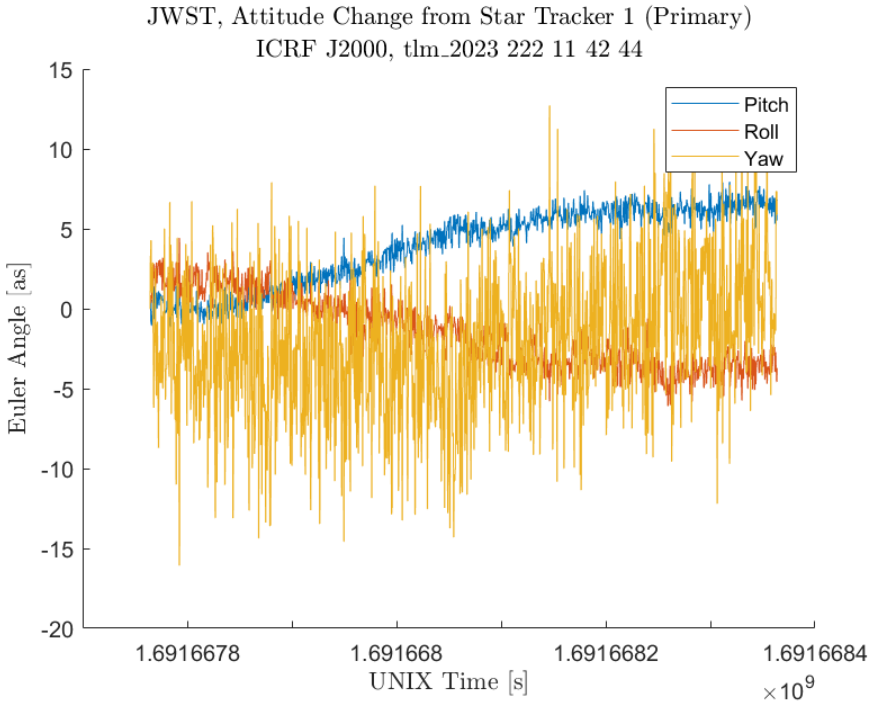

Figure 4. Change in unfiltered star tracker attitude data.

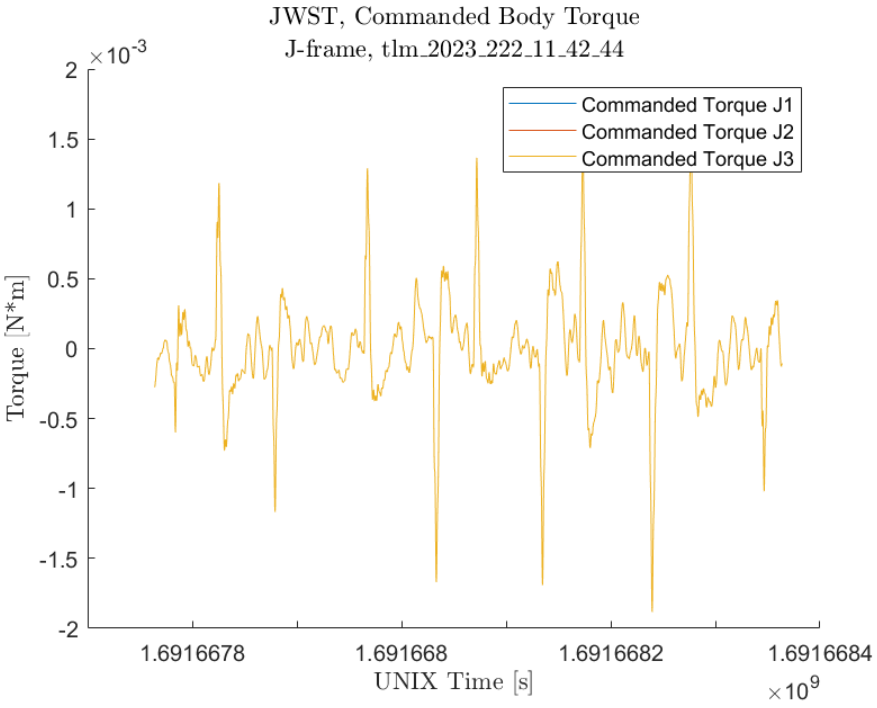

Figure 5. JWST commanded body torque.

docking (RPOD) of bodies whose masses are within a few orders of magnitude of one another, or for identifying oscillating appendages or fuel slosh. Future work may seek to address current gaps in this work, specifically the robustness of the VI against high angular velocities and the unscented Kalman filtering (UKF) of the telemetry data.

REFERENCES

[1] M. M. Wittal, B. W. Asher, and M. Nazari, "Autonomous RPOD For Arbitrarily Configured Spacecraft with Anomaly Detection," *AAS/AIAA Astrodynamics Specialist Conference*, 2024.

[2] M. A. Clark, A. Pensado, C. A. Jones, M. L. Grande, and E. Judd, "How the Allocation of Lander Functions Impacts Human Lunar Exploration Architecture Propellant Demands," *AIAA Scitech Forum*, 2021, 10.2514/6.2021-0627.

[3] M. Fagetti, B. McCann, M. Nazari, M. Wittal, and J. Smith, "Mass and Inertia Property Estimation on TSE(3) in the Presence of a Sloshing Liquid," *AAS/AIAA Space Flight Mechanics Meeting*, 2023.

[4] T. Lee, M. Leok, and N. H. McClamroch, "Lie Group Variational Integrators for the Full Body Problem," *Computational Methods in Applied Mechanics and Engineering*, Vol. 196, No. 8, 2005, doi: 10.1016/j.cma.2007.01.017.